Markedly enhanced absorption and direct radiative forcing of black carbon under polluted urban environments

Jianfei Peng[a,1], Min Hu[a,2], Song Guo[a,b,1], Zhuofei Du[a], Jing Zheng[a], Dongjie Shang[a], Misti Levy Zamora[b], Limin Zeng[a], Min Shao[b], Yu-Sheng Wu[a], Jun Zheng[b,3], Yuan Wang[c], Crystal R. Glen[b,4], Donald R. Collins[b], Mario J. Molina[d,2], and Renyi Zhang[a,b,2]

[a]State Key Joint Laboratory of Environmental Simulation and Pollution Control, College of Environmental Sciences and Engineering, Peking University, 100871 Beijing, China; [b]Department of Atmospheric Sciences, Texas A&M University, College Station, TX 77843; [c]Jet Propulsion Laboratory, California Institute of Technology, Pasadena, CA 91125; and [d]Department of Chemistry and Biochemistry, University of California, San Diego, La Jolla, CA 92093

Contributed by Mario J. Molina, February 16, 2016 (sent for review October 2, 2015; reviewed by Zhanqing Li and Yangang Liu)

Black carbon (BC) exerts profound impacts on air quality and climate because of its high absorption cross-section over a broad range of electromagnetic spectra, but the current results on absorption enhancement of BC particles during atmospheric aging remain conflicting. Here, we quantified the aging and variation in the optical properties of BC particles under ambient conditions in Beijing, China, and Houston, United States, using a novel environmental chamber approach. BC aging exhibits two distinct stages, i.e., initial transformation from a fractal to spherical morphology with little absorption variation and subsequent growth of fully compact particles with a large absorption enhancement. The timescales to achieve complete morphology modification and an absorption amplification factor of 2.4 for BC particles are estimated to be 2.3 h and 4.6 h, respectively, in Beijing, compared with 9 h and 18 h, respectively, in Houston. Our findings indicate that BC under polluted urban environments could play an essential role in pollution development and contribute importantly to large positive radiative forcing. The variation in direct radiative forcing is dependent on the rate and timescale of BC aging, with a clear distinction between urban cities in developed and developing countries, i.e., a higher climatic impact in more polluted environments. We suggest that mediation in BC emissions achieves a cobenefit in simultaneously controlling air pollution and protecting climate, especially for developing countries.

black carbon | absorption | air quality | radiative forcing | climate

Black carbon (BC) particles, produced from incomplete fossil fuel combustion and biomass burning, are ubiquitous in the atmosphere and have profound impacts on air quality and climate (1–4). As a key short-lived climate forcer, the magnitude of BC direct radiative forcing (DRF) is dependent on the mixing state, i.e., whether particles are externally or internally mixed with other aerosol types (5, 6), and atmospheric aging by coating with secondary aerosol constituents (such as organics and sulfate) enhances the mass absorption cross-section (MAC) (5–9). Previous laboratory studies conducted under controlled experimental conditions yielded a broad range of MAC enhancements from 1.05 to 3.50, varying with the diameter, morphology, and coating of BC particles (7–15). On the other hand, a field measurement indicated a negligible absorption enhancement of ambient BC particles under a variable mixing state (16). In addition, BC aging and absorption enhancement also strongly impact visibility and atmospheric stability.

Few direct measurements have been conducted to capture aging and quantify the related absorption variation of BC particles under ambient conditions. In particular, atmospheric measurements at fixed sites are affected by transport, local emissions, and chemistry, and quantification of the evolution in the BC properties (such as morphology, mixing state, and absorption and scattering coefficients) during aging involves complex decoupling of the various processes (17). To overcome the deficiencies in field measurements, we developed a novel quasi-atmospheric aerosol evolution study (QUALITY) chamber (Fig. S1), by mimicking the ambient gaseous concentrations without the presence of ambient aerosols but introducing seed BC particles, to evaluate the aging and variation in the particle properties under atmospheric conditions (see *Materials and Methods*). The experiments were performed during May–June 2009 in Houston and August–October 2013 in Beijing, representative of the typical ambient urban conditions in developed and developing countries, respectively (2, 17–19).

Results and Discussion

Morphology Variation. The change in the mass equivalent diameter (ΔD_{me} or total coating thickness) of BC particles due to exposure to ambient air in the presence of sunlight ranges from 32 nm to 152 nm during a period of 2–5 h in Beijing (Fig. 1). The variation in the total coating thickness is closely correlated with the photolysis efficiency (Fig. S2), indicating the importance of

Significance

Although black carbon (BC) represents a key short-lived climate forcer, its direct radiative forcing remains highly uncertain. The available results from available studies of absorption enhancement of BC particles during atmospheric aging are conflicting. Using a novel environmental chamber method, we have, for the first time to our knowledge, quantified the aging and variation in the optical properties of BC particles under ambient urban conditions representative of developed and developing countries. Our results indicate that BC under polluted urban environments could contribute significantly to both pollution development and large positive radiative forcing, implying that reduction of BC emissions under polluted environments achieves a cobenefit in simultaneously controlling air pollution and protecting climate, especially for developing countries.

Author contributions: R.Z. designed research; J.P., S.G., Z.D., Jing Zheng, D.S., Y.-S.W., Jun Zheng, Y.W., C.R.G., and R.Z. performed research; M.H., L.Z., M.S., D.R.C., M.J.M., and R.Z. contributed new reagents/analytic tools; M.H., S.G., M.L.Z., M.J.M., and R.Z. analyzed data; and J.P., M.H., M.J.M., and R.Z. wrote the paper.

Reviewers: Z.L., University of Maryland, College Park; and Y.L., Brookhaven National Laboratory.

The authors declare no conflict of interest.

Freely available online through the PNAS open access option.

See Commentary on page 4243.

[1]J.P. and S.G. contributed equally to this work.

[2]To whom correspondence may be addressed. Email: renyi-zhang@tamu.edu, minhu@pku.edu.cn, or mjmolina@ucsd.edu.

[3]Present address: Jiangsu Key Laboratory of Atmospheric Environment Monitoring and Pollution Control, Nanjing University of Information Science & Technology, Nanjing 210044, China.

[4]Present address: Sandia National Laboratories, Albuquerque, NM 87185.

This article contains supporting information online at www.pnas.org/lookup/suppl/doi:10.1073/pnas.1602310113/-/DCSupplemental.

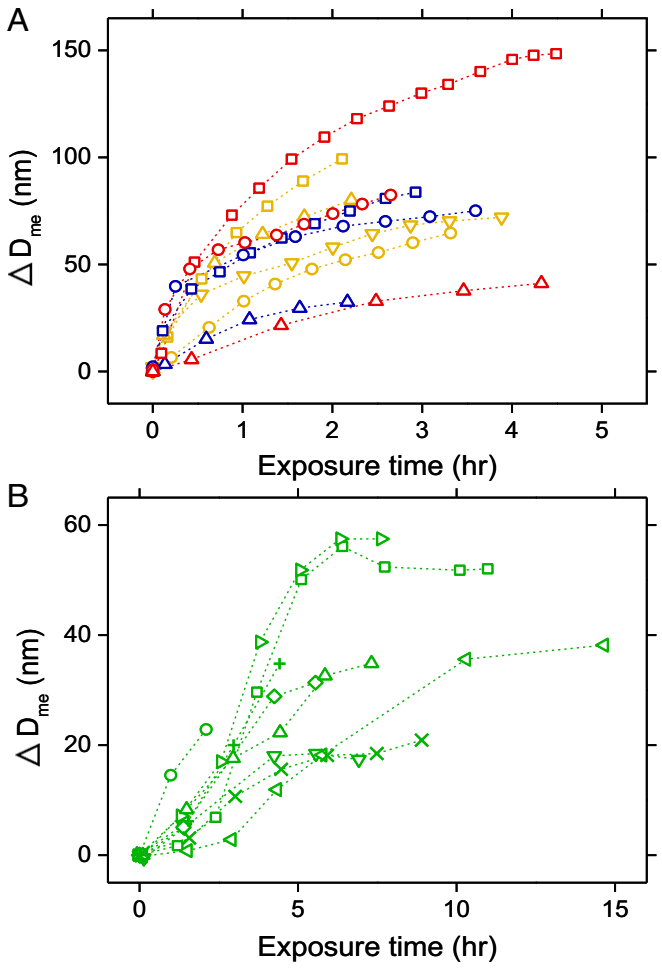

Fig. 1. Distinct BC aging in Beijing and Houston. Temporal variation in the BC mass equivalent diameter (ΔD_{me} or total coating thickness) as a function of exposure time to ambient air in Beijing (*A*) and Houston (*B*). The yellow, blue, and red symbols in *A* represent experiments conducted with the initial BC mobility diameters ($D_{m,0}$) of about 100 nm, 150 nm, and 220 nm, respectively. The green symbols in *B* represent experiments conducted with the initial mobility diameter of about 100 nm. The symbols denote measurements conducted on different days, and the dashed lines connect the measurements of the same experiments.

photochemical production of the BC coating materials. In contrast, BC particles exhibit an appreciably slower growth in Houston, with the total coating thickness from 10 nm to 60 nm during a period of 4–10 h. The more efficient BC growth in Beijing is attributable to higher concentrations of gaseous aerosol precursors (17), most noticeably anthropogenic volatile organic compounds (VOCs); during our measurement periods, the peak ambient xylene and toluene concentrations exceeded 10 ppb in Beijing (18), but were typically less than a few parts per billion in Houston (19). In addition, the average ambient mass concentrations of fine particulate matter (particles with a diameter smaller than 2.5 μm or $PM_{2.5}$) during our experiments were 36 $\mu g \cdot m^{-3}$ and 11 $\mu g \cdot m^{-3}$ in Beijing and Houston, respectively, corresponding to typical clean conditions in both locations (17). Measurements of the particle compositions by an Aerosol Mass Spectrometer (AMS) reveal a large mass fraction of secondary organics as the coating materials (great than 90%), consistent with a chemical constituent dominated by organics during the initial stage of haze development in Beijing (18). Throughout the pollution period in Beijing, the contributions of organic and inorganic (i.e., sulfate and nitrate) species to the particle mass concentrations have been found to decrease and increase (18), respectively, with the latter likely attributable to an increasing importance of aqueous chemistry (2).

BC aging leads to a large variation in the particle morphology, depicted in the evolutions of the effective density (ρ_{eff}) and dynamic shape factor (DSF) (Fig. 2). For three initial mobility diameters (D_m) of about 100 nm, 150 nm, and 200 nm in Beijing, the values of ρ_{eff} and DSF for fresh BC particles are 0.46 $g \cdot cm^{-3}$, 0.34 $g \cdot cm^{-3}$, and 0.25 $g \cdot cm^{-3}$ and 2.2, 2.5, and 2.8, respectively, indicating fractal aggregates with chain-like branches (10, 11, 20–22) and a more fractal morphology for a larger size. Our estimated fractal dimension of 2.25 for fresh BC particles is similar to those in the previous studies (13, 22, 23). When the total coating thickness reaches 30 nm, 40 nm, and 60 nm for the three initial mobility diameters (i.e., 100 nm, 150 nm, and 200 nm, respectively), DSF decreases nearly to unity (Fig. 2), indicating complete transformation from highly fractal to fully compact and spherical BC particles (10, 11). The corresponding ρ_{eff} value increases to 1.4 $g \cdot cm^{-3}$ after the BC compaction, comparable to the coating material density of 1.3–1.4 $g \cdot cm^{-3}$ estimated from the AMS measurements. When BC particles are fully compact and become spherical, the total coating thickness equals half of the initial mass equivalent diameter ($D_{me,0}$) for the three particle sizes, corresponding to a coating fraction ($\Delta D_{me}/D_{me,0}$) of 0.5.

Absorption Enhancement. The measured MAC in Beijing exhibits little change for a coating fraction of less than 0.5, but a large absorption enhancement occurs for a coating fraction of greater than 0.5 (Fig. 3). For the wavelengths of 405 nm and 532 nm, the largest absorption enhancement by a factor of 2.4 is obtained for 150-nm and 220-nm particles. The measured MAC in Houston exhibits little change with a small coating fraction (<0.5). During the initial morphology change, a thin dielectric coating layer hinders the interaction of electromagnetic (EM) coupling between neighboring spherules, and the internal spherules are shielded by the outer ones, likely responsible for little absorption enhancement (8, 24). For fully compact BC particles, efficient EM coupling between neighboring spherules contributes to an enhanced MAC, in addition to the lensing effect (15, 24). The Mie theory with the core–shell assumption for homogeneous spherical particles (25, 26) is used to calculate MAC. The measured and calculated absorption enhancements show comparable values for a large coating fraction (>0.5) at both wavelengths (Fig. 3), but the Mie calculation yields absorption enhancement even for a coating fraction smaller than 0.5, because of the lensing effect (8).

Our measurements demonstrate that the BC morphology variation during atmospheric aging is characterized by two distinct stages, which are delineated by the coating fraction or DSF, i.e., the initial conversion from a highly fractal structure to a spherical shape with the coating fraction < 0.5 or DSF > 1 and the subsequent growth of the fully compact particles with the coating fraction > 0.5 or DSF ≈ 1 (Fig. 4). For fractal BC particles, there is negligible absorption variation, whereas compact BC particles exhibit noticeably enhanced MAC, with the maximum absorption enhancement factor of 2.4 for a coating fraction of unity. BC particles undergo rapid morphology modification in Beijing (2.3 h) and subsequently exhibit large absorption amplification (4.6 h). In contrast, achieving similar morphology and absorption variations requires much longer times (9 h and 18 h, respectively) in Houston.

The average positive BC DRF is predicted to be 0.64 (from 0.25 to 1.09) $W \cdot m^{-2}$ from global climate models (1); BC particles are typically categorized into two distinct states of external (fresh) and internal (fully aged) mixing with correspondingly predetermined MAC values, and the conversion time between the two states is fixed at about 24 h (12, 27). Our measured maximum absorption enhancement factor of 2.4 in Beijing is larger than those commonly adopted in global climate models (12, 27–29). To assess the climatic implications of BC aging, our measured absorption enhancement is used to estimate DRF on

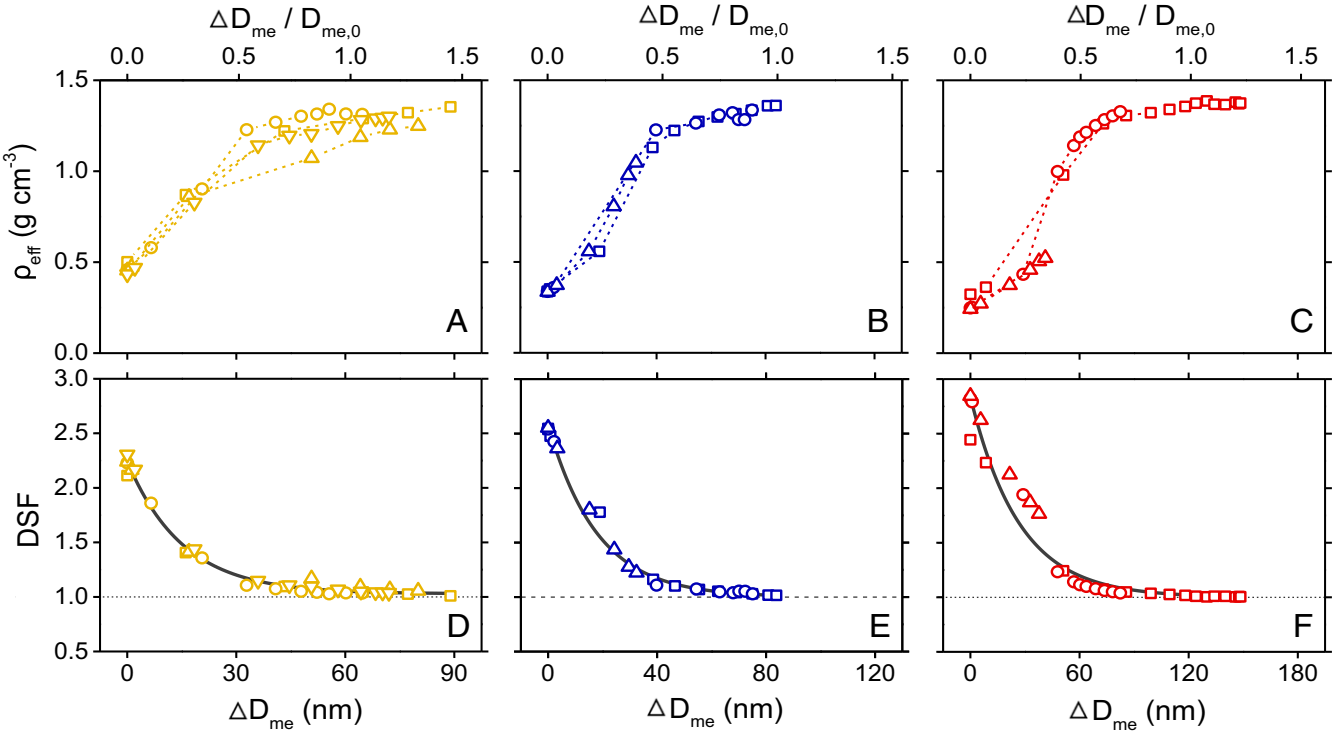

Fig. 2. BC morphological evolution. The ρ_{eff} (*A*–*C*) and DSF (*D*–*F*) as a function the total coating thickness (ΔD_{me}, bottom axis) or coating fraction ($\Delta D_{me}/D_{me,0}$, top axis) with the initial mobility diameters of about 100 nm (*A* and *D*), 150 nm (*B* and *E*), and 220 nm (*C* and *F*) conducted in Beijing. The black curves in *D*–*F* correspond to fitting through the DSF values. The symbols are similar to those in Fig. 1*A*.

the basis of simulations from the previous global climate models (12). The DRF difference between fully aged and fresh BC particles increases by 0.45 W·m^{-2} (Table S1), with a range of 0.21–0.80 W·m^{-2} reflecting the uncertainty in the model simulations (Fig. 4).

Atmospheric Implications. Our results indicate that aging of BC particles under polluted urban environments exerts large impacts on air quality and climate (1, 2). For example, the enhanced optical properties of BC strongly influence visibility, air quality, and weather (3, 24, 30). Light absorption and scattering by BC lead to stabilization of the atmosphere, because of cooling at the surface and warming aloft (24). A stable atmospheric profile restricts vertical transport, which has a negative impact on air quality by accumulation of gaseous and particulate matter pollutants within the planetary boundary layer (PBL).

We illustrate distinct aging rates and resulting absorption enhancements of BC particles between Beijing and Houston, which are representative of those for urban cities in developing and developed countries (2). In both locations, BC particles exhibit noticeable morphology variations, but aging occurs much more efficiently in Beijing than in Houston. Our measured rapid aging and growth of BC particles in Beijing are consistent with the previous results by Guo et al., showing enormously efficient secondary photochemical growth of fine aerosols during the initial stage of haze development that is attributable to highly elevated levels of gaseous pollutants (18). The rapid morphology modification in Beijing (2.3 h) leads to large absorption amplification within a short time (4.6 h), in contrast to those for achieving similar morphology and absorption variations in Houston (9 h and 18 h, respectively). Hence, the rapid aging and largely enhanced absorption of BC particles (i.e., an absorption enhancement factor of 2.4 within a few hours) could contribute importantly to atmospheric stabilization and diminished diurnal PBL variation (2, 17, 18), exacerbating formation of severe haze events.

Currently, the results of absorption enhancement of BC particles during atmospheric aging from available experimental, theoretical, modeling, and field studies are conflicting, leading to large uncertainty in global radiative transfer calculations (12). Our measured absorption enhancement illustrates that the positive DRF of BC particles is highly dependent on the rate and the timescale of aging, which are currently unaccounted for in global climate models. Our results also provide a plausible reconciliation of the conflicting results of largely variable absorption enhancement and DRF of BC particles in the previous studies, i.e., an underestimated DRF in heavily polluted regions of East and South Asia predicted from a global climate model (29) but a low absorption enhancement measured in California (16). In addition, light absorption can be also enhanced by mixed BC and brown carbon particles (31).

Finally, our results suggest a distinction for BC particles between urban cities in developed and developing countries, i.e., a larger climatic impact in more polluted environments. It is commonly believed that improving air quality by reducing fine PM may counteract climate protection, because of the negative direct and indirect radiative forcings by nonabsorbing aerosols, in contrast to warming imposed by greenhouse gases (1). Our findings indicate that BC under polluted urban environments could contribute significantly to both pollution development and large positive radiative forcing, indicating that mitigation in BC emissions achieves a cobenefit in simultaneously controlling air pollution and protecting climate, especially for developing countries (1, 2, 32–34).

Conclusions

Using a novel environmental chamber approach, we have quantified the aging and variations in the morphology and optical properties of BC particles under ambient conditions in Beijing, China, and Houston, United States. Our results show that BC aging exhibits two distinct stages, i.e., initial transformation

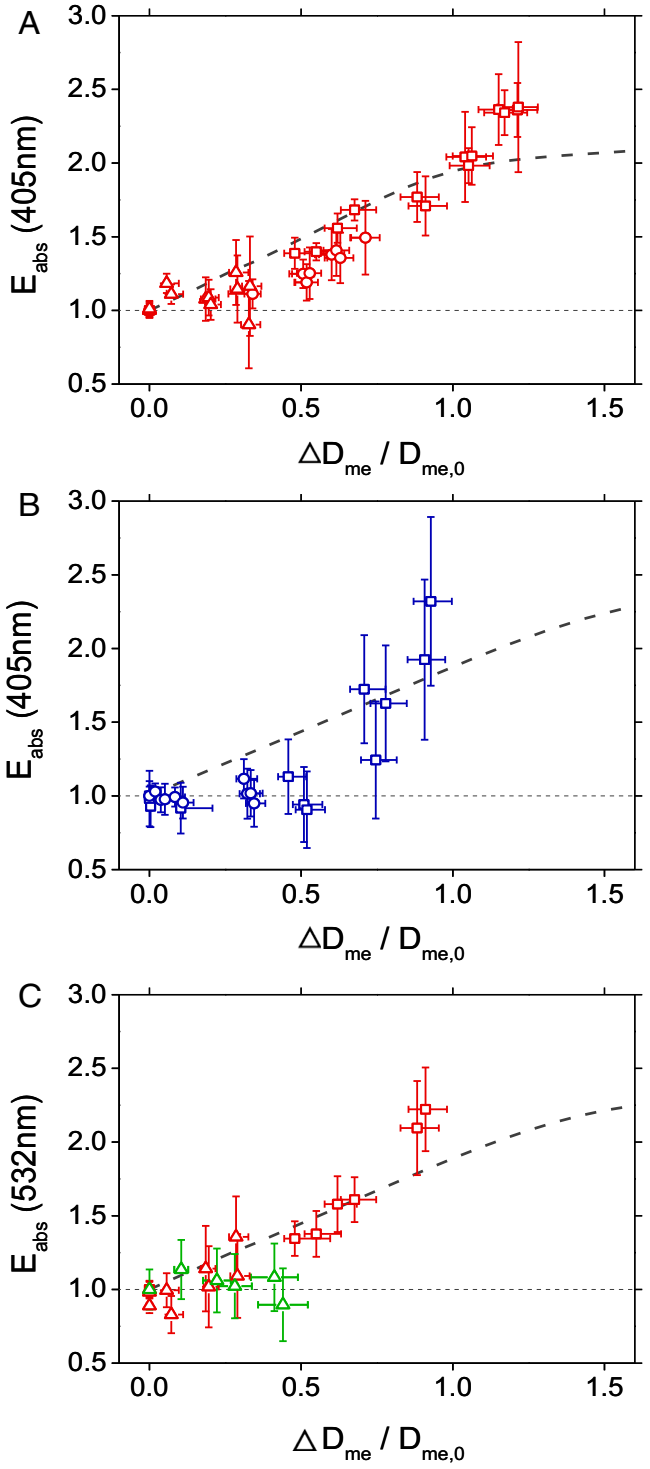

Fig. 3. BC absorption enhancement. Measured (symbols) and modeled (dashed line) absorption enhancement (E_{abs}), defined by the ratio of the MAC values of aged to fresh BC particles, as a function of the coating fraction ($\Delta D_{me}/D_{me,0}$): (*A*) absorption enhancement with an initial mobility diameter of about 220 nm at the wavelength of 405 nm in Beijing, (*B*) absorption enhancement for about 150-nm particles at the wavelength of 405 nm in Beijing, and (*C*) comparison of absorption enhancements in Beijing (220-nm particles, red) and Houston (100-nm particles, green) at the wavelength of 532 nm. The error bars represent 1 SD considering the random and systematic errors. Calculated absorption enhancements with the consideration of the particle size distribution using the core–shell Mie theory are shown as the dash lines. The symbols are similar to those in Figs. 1 and 2.

from a fractal to spherical morphology with little absorption variation and subsequent growth of fully compact particles with a large absorption enhancement. On the basis of our measurements, we have estimated the timescales of 2.3 h and 4.6 h, respectively, in Beijing to achieve complete morphology modification and an absorption amplification factor of 2.4 for BC particles, compared with 9 h and 18 h, respectively, in Houston. Our quantified BC morphology and absorption variations during aging are broadly applicable to diverse urban environments for improvement in radiative transfer calculations. Hence, our results have important implications for the assessments of the impacts of BC on air quality and climate.

Materials and Methods

The QUALITY chamber was divided into a lower flow chamber, where ambient air was pulled through continuously, and an upper reaction chamber, where the aging experiments were conducted (35). The two chambers were separated by a 5-μm-thick membrane, which allowed unimpeded penetration of ambient gases at a steady flow rate but filtered out ambient particles from the lower to upper chambers. The upper reaction chamber (1.2 m^3) was made of PFA (perfluoroalkoxy) Teflon for efficient UV light transmission. Monodisperse fresh BC particles produced from incomplete combustion (10, 11) were introduced into the reaction chamber and exposed to sunlight. For example, the initial size and number concentration of BC particles introduced to the upper reaction chamber in Beijing were 195–224 nm and 800–4,200 particles·cm^{-3}, respectively, corresponding to a mass concentration in the range of 0.3–12 μg·m^{-3}. A suite of high time resolution state-of-the-art aerosol instruments simultaneously measured a comprehensive set of BC properties throughout the BC aging process, including the particle diameter, mass, chemical composition, and optical coefficients (Fig. S1). The field measurements in Beijing were conducted on the campus of Peking University. The descriptions of the field sites and periods as well as ambient measurements in Beijing and Houston were provided previously (18, 19).

An integrated PM monitoring system, consisting of tandem differential mobility analyzer and aerosol particle mass analyzer (APM) was used to measure the aerosol mass–size relation, including the effective density, volatility, hygroscopicity, and DSF (18, 19). Aerosol optical properties were measured using three Photoacoustic Extinctiometers (PAX; DMT Inc.) in Beijing and a combined Cavity Ring Down Spectrometer (CRDS) and a nephelometer (3563; TSI, Inc.) in Houston (18, 19). The PAX used in situ photoacoustic technology to measure BC absorption. A laser beam directed through the aerosol stream was modulated at the resonant frequency of the acoustic chamber. Absorbing particles were heated up and quickly transferred heat to the surrounding air. The periodic heating produced pressure waves that were detected with a sensitive microphone. The system then determined the resonator quality factor and resonance frequency, which were needed to quantitatively determine aerosol light absorption. The laser wavelengths of the PAX are 405 nm, 532 nm, and 870 nm. The instruments were calculated with PSL (Polystyrene Latex Spheres) spheres and Aquadag soot particles, and zero check was performed automatically every 10 min. The CRDS measures aerosol extinction coefficients at 532 nm. During each experiment, an 11-ns 532-nm light pulse from a Q-switched laser was introduced into a stainless steel cell formed by two mirrors that had 99.9985% reflectivity and an aerosol inlet in the center. Light exiting in the cavity was detected with a photomultiplier. The extinction coefficient was then calculated by nonlinear fitting of the averaged decay data.

The Mie theory with the core–shell assumption for homogeneous spherical particles was used to calculate MAC (25). The core–shell Mie model requires several input parameters, e.g., the size distribution of BC particles, the sizes of the inner BC core and outer shell, the refractive indexes of the BC core and coating materials (26). Because the core–shell Mie model assumes that all particles are compact spheres and both the BC core and outer shell are homogeneous, the core of aged BC particles is represented as the mass equivalent diameter (D_{me}) of fresh BC particle. The D_{me} of BC particles for the entire size range is calculated from

$$D_{me} = \sqrt[3]{\frac{6k}{\pi\rho_m}} D_m^{D_f/3} \quad [1]$$

where D_f is the fractal dimension for fresh BC particles, which is determined to be 2.25 in this study, and k is a constant. For aged BC particles, the size distribution of the core (D_{core}) is equal to the size distribution of the mass

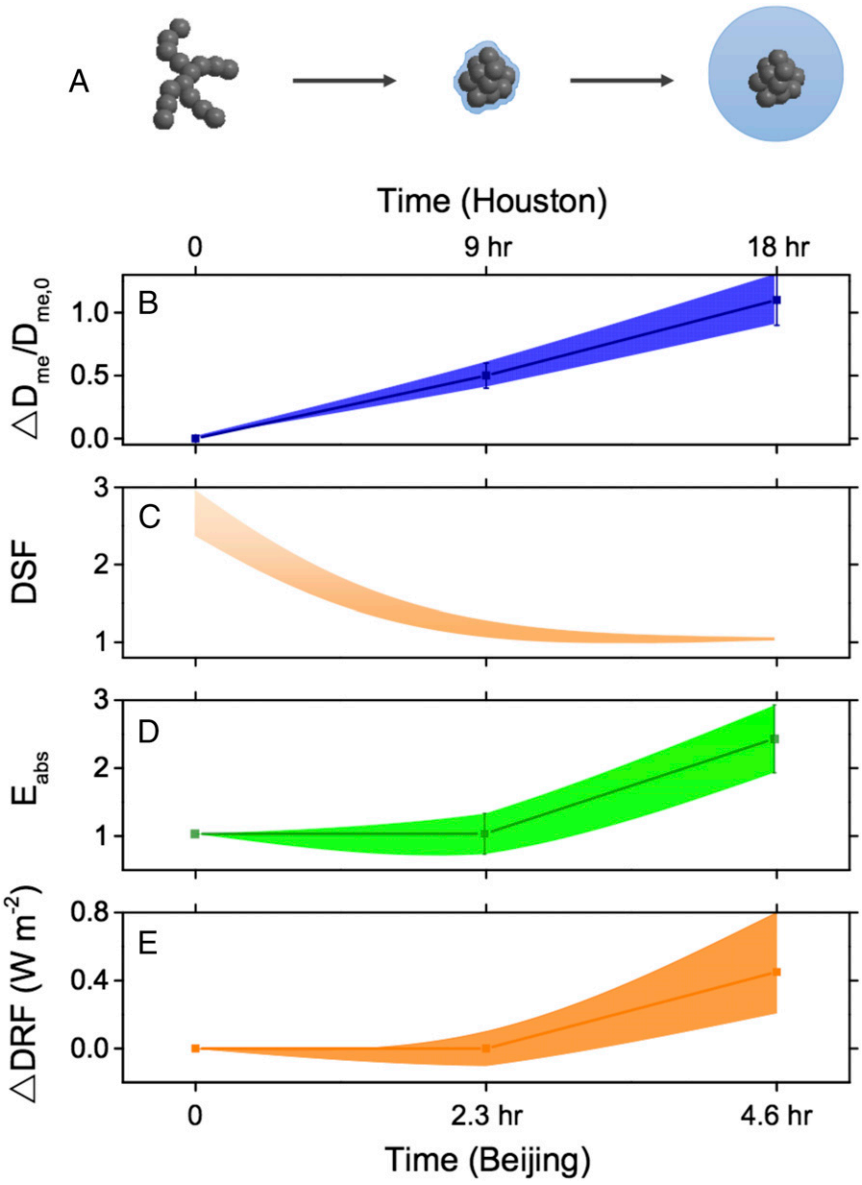

Fig. 4. BC aging and DRF. A two-stage morphology variation of BC particles during atmospheric aging, characterized by initial transformation from a fractal to spherical morphology and the subsequent growth of fully compact particles (*A*), and evolutions in the particle properties, i.e., (*B*) the coating fraction ($\Delta D_{me}/D_{me,0}$), (*C*) DSF, (*D*) absorption enhancement (E_{abs}), and (*E*) the positive DRF difference between fully aged and fresh BC particles (ΔDRF). The timescale of aging is estimated for BC particles with $D_{me,0}$ = 120 nm using our measured average growth rates under the ambient conditions in Beijing (bottom axis) and Houston (top axis).

equivalent diameter of fresh BC particle ($D_{me,0}$). Thus, with the assumption that the increases of mass equivalent diameter ($\Delta D_{me,}$) are identical for BC particles within the entire size range, the mass equivalent diameter of aged BC particle is calculated by adding $D_{me,0}$ and $\Delta D_{me,0}$. The refractive index of fresh BC particles and the coating material used in this study are 1.91 + 0.71i and 1.55 + 0i, respectively. For comparison, Bond et al. suggested a refractive index value of 1.95 + 0.79i for pure BC (12). In our study, the generated BC particles were measured to contain about 80% pure BC and 20% organic matter. Thus, the refractive index of fresh BC particles was estimated to be 1.91 + 0.71i. The refractive index of coating material was measured in a parallel experiment without the injection of BC particles. In this experiment, new particles were produced by nucleation without seeded aerosols inside the chamber (36). By measuring the scattering and absorption coefficients, size distribution, and density of the particles formed, the refractive index was calculated to be 1.55 + 0i at the wavelength of 405 nm. Because the chemical composition of newly formed particles was similar to the coating material of the BC aging experiments, this refractive index value was considered to be representative of that of the coating material. The analysis of particle composition indicates the presence of dominant organic species as the coating materials in our experiments, formed from photochemical oxidation of VOCs (37–40). Because urban fine PM also contains a large portion of inorganic species (such as sulfate, nitrate, and ammonium), our measured BC aging rates and variations in the optical properties likely represent the lower limits under ambient conditions (17, 41). Also, note that the change in effective density implies change in refractive index. It has been suggested that the mixing rule (e.g., linear mixing and Lorentz–Lorenz mixing rule) may be appropriate to estimate the refractive index for an aerosol mixture (42).

ACKNOWLEDGMENTS. We thank Wei Hu and Zhaoheng Gong for their assistance with the AMS data analysis, Wentai Chen and Yue Li for providing VOCs data, and Nan Ma for providing the core–shell code for the Mie calculation. This work was supported by National Natural Science Foundation of China (Grants 91544214 and 21190052), the National Basic Research Program, China Ministry of Science and Technology (Grant 2013CB228503), National Natural Science Foundation of China (Grant 21190052), and the China Ministry of Environmental Protection's Special Funds for Scientific Research on Public Welfare (Grant 20130916). R.Z. acknowledges support from the Robert A. Welch Foundation (Grant A-1417) and Houston Advanced Research Center.

1. Stocker TF, et al., eds (2013) *Intergovernmental Panel on Climate Change. Climate Change 2013: The Physical Science Basis. Contribution of Working Group I to the Fifth Assessment Report of the Intergovernmental Panel on Climate Change* (Cambridge Univ Press, New York).
2. Zhang R, et al. (2015) Formation of urban fine particulate matter. *Chem Rev* 115(10): 3803–3855.
3. Fan J, et al. (2008) Effects of aerosol optical properties on deep convective clouds and radiative forcing. *J Geophys Res* 113(D08):D08209.
4. Myhre G (2009) Consistency between satellite-derived and modeled estimates of the direct aerosol effect. *Science* 325(5937):187–190.
5. Jacobson MZ (2001) Strong radiative heating due to the mixing state of black carbon in atmospheric aerosols. *Nature* 409(6821):695–697.
6. Ramanathan V, Carmichael G (2008) Global and regional climate changes due to black carbon. *Nat Geosci* 1(4):221–227.
7. Shiraiwa M, Kondo Y, Iwamoto T, Kita K (2010) Amplification of light absorption of black carbon by organic coating. *Aerosol Sci Technol* 44(1):46–54.
8. Khalizov AF, Xue H, Wang L, Zheng J, Zhang R (2009) Enhanced light absorption and scattering by carbon soot aerosol internally mixed with sulfuric acid. *J Phys Chem A* 113(6):1066–1074.
9. Schnaiter M (2005) Absorption amplification of black carbon internally mixed with secondary organic aerosol. *J Geophys Res* 110(D19):D19204.
10. Khalizov AF, et al. (2013) Role of OH-initiated oxidation of isoprene in aging of combustion soot. *Environ Sci Technol* 47(5):2254–2263.
11. Qiu C, Khalizov AF, Zhang R (2012) Soot aging from OH-initiated oxidation of toluene. *Environ Sci Technol* 46(17):9464–9472.
12. Bond TC, et al. (2013) Bounding the role of black carbon in the climate system: A scientific assessment. *J Geophys Res* 118(11):5380–5552.
13. Saathoff H, et al. (2003) Coating of soot and $(NH_4)_2SO_4$ particles by ozonolysis products of α-pinene. *J Aerosol Sci* 34(10):1297–1321.
14. Xue H, Khalizov AF, Wang L, Zheng J, Zhang R (2009) Effects of dicarboxylic acid coating on the optical properties of soot. *Phys Chem Chem Phys* 11(36):7869–7875.
15. Bueno PA, et al. (2011) Photoacoustic measurements of amplification of the absorption cross section for coated soot aerosols. *Aerosol Sci Technol* 45(10):1217–1230.
16. Cappa CD, et al. (2012) Radiative absorption enhancements due to the mixing state of atmospheric black carbon. *Science* 337(6098):1078–1081.
17. Zhang R, Guo S, Levy Zamora M, Hu M (2015) Reply to Li et al.: Insufficient evidence for the contribution of regional transport to severe haze formation in Beijing. *Proc Natl Acad Sci USA* 112(21):E2741.
18. Guo S, et al. (2014) Elucidating severe urban haze formation in China. *Proc Natl Acad Sci USA* 111(49):17373–17378.
19. Levy ME, et al. (2013) Measurements of submicron aerosols in Houston, Texas during the 2009 SHARP field campaign. *J Geophys Res* 118(18):10518–10534.
20. Xue H, Khalizov AF, Wang L, Zheng J, Zhang R (2009) Effects of coating of dicarboxylic acids on the mass-mobility relationship of soot particles. *Environ Sci Technol* 43(8):2787–2792.
21. Khalizov AF, et al. (2009) Formation of highly hygroscopic aerosols upon internal mixing of airborne soot particles with sulfuric acid vapor. *J Geophys Res* 114(D05):D05208.
22. Zhang R, et al. (2008) Variability in morphology, hygroscopicity, and optical properties of soot aerosols during atmospheric processing. *Proc Natl Acad Sci USA* 105(30):10291–10296.
23. Khalizov AF, et al. (2012) Characterization of soot aerosol produced from combustion of propane in a shock tube. *Aerosol Sci Technol* 46(8):925–936.
24. Wang Y, Khalizov A, Levy M, Zhang R (2013) New Directions: Light absorbing aerosols and their atmospheric impacts. *Atmos Environ* 81(4):713–715.
25. Bohren CF, Huffman DR (1983) *Absorption and Scattering of Light by Small Particles* (Wiley, New York).
26. He C, et al. (2015) Variation of the radiative properties during black carbon aging: Theoretical and experimental intercomparison. *Atmos Chem Phys* 15(20): 11967–11980.
27. Koch D, Schulz M, Kinne S, Mcnaughton C (2009) Evaluation of black carbon estimations in global aerosol models. *Atmos Chem Phys* 9(22):9001–9026.
28. Myhre G, et al. (2013) Radiative forcing of the direct aerosol effect from AeroCom Phase II simulations. *Atmos Chem Phys* 13(4):1853–1877.
29. Chung CE, Ramanathan V, Decremer D (2012) Observationally constrained estimates of carbonaceous aerosol radiative forcing. *Proc Natl Acad Sci USA* 109(29): 11624–11629.
30. Wang Y, et al. (2011) Long-term impacts of aerosols on precipitation and lightning over the Pearl River Delta megacity area in China. *Atmos Chem Phys* 11(23): 12421–12436.
31. Liu S, et al. (2015) Enhanced light absorption by mixed source black and brown carbon particles in UK winter. *Nat Commun* 6:8435.
32. Zhang R, Li G, Fan J, Wu DL, Molina MJ (2007) Intensification of Pacific storm track linked to Asian pollution. *Proc Natl Acad Sci USA* 104(13):5295–5299.
33. Wang Y, Zhang R, Saravanan R (2014) Asian pollution climatically modulates midlatitude cyclones following hierarchical modelling and observational analysis. *Nat Commun* 5:3098.
34. Wang Y, et al. (2014) Assessing the effects of anthropogenic aerosols on Pacific storm track using a multiscale global climate model. *Proc Natl Acad Sci USA* 111(19): 6894–6899.
35. Glen C (2010) Observations of secondary organic aerosol production and soot aging under atmospheric conditions using a novel new environmental aerosol chamber. PhD dissertation (Texas A&M Univ, College Station, TX).
36. Zhang R, Khalizov A, Wang L, Hu M, Xu W (2012) Nucleation and growth of nanoparticles in the atmosphere. *Chem Rev* 112(3):1957–2011.
37. Zhao J, Zhang R, Misawa K, Shibuya K (2005) Experimental product study of the OH-initiated oxidation of m-xylene. *J Photoch Photobio A* 176(1-3):199–207.
38. Suh I, Zhang R, Molina LT, Molina MJ (2003) Oxidation mechanism of aromatic peroxy and bicyclic radicals from OH-toluene reactions. *J Am Chem Soc* 125(41):12655–12665.
39. Zhang D, Zhang R, Park J, North SW (2002) Hydroxy peroxy nitrites and nitrates from OH initiated reactions of isoprene. *J Am Chem Soc* 124(32):9600–9605.
40. Lei W, Zhang R, McGivern WS, Derecskei-Kovacs A, North SW (2001) Theoretical study of $OH-O_2-$isoprene peroxy radicals. *J Phys Chem* 105(2):471–477.
41. Li G, Wang Y, Zhang R (2008) Implementation of a two-moment bulk microphysics scheme to the WRF model to investigate aerosol-cloud interaction. *J Geophys Res* 113(D11):D15211.
42. Liu Y, Daum PH (2008) Relationship of refractive index to mass density and self-consistency of mixing rules for multicomponent mixtures like ambient aerosols. *J Aerosol Sci* 39(11):974–986.